REVIEW

doi:10.1038/nature13784

Instrumentation for the detection and characterization of exoplanets

Francesco Pepe[1], David Ehrenreich[1] & Michael R. Meyer[2]

In no other field of astrophysics has the impact of new instrumentation been as substantial as in the domain of exoplanets. Before 1995 our knowledge of exoplanets was mainly based on philosophical and theoretical considerations. The years that followed have been marked, instead, by surprising discoveries made possible by high-precision instruments. Over the past decade, the availability of new techniques has moved the focus of research from the detection to the characterization of exoplanets. Next-generation facilities will produce even more complementary data that will lead to a comprehensive view of exoplanet characteristics and, by comparison with theoretical models, to a better understanding of planet formation.

Astrometry is the most ancient technique of astronomy. It is, therefore, not surprising that the first (unconfirmed) detection of an extrasolar planet arose through this technique[1]. In 1984, another detection of a planetary-mass object around the nearby star VB 8 was reported, this time using speckle interferometry[2], but subsequent attempts to locate it were unsuccessful. It was finally Doppler velocimetry that delivered the first unambiguous detection of a very low-mass companion (HD 114762b[3]). However, because its minimum mass (11 M_J) is near the upper limit of the planetary mass range, the discoverers cautiously announced it was a brown dwarf. In 1992, a handful of bodies of terrestrial mass were found[4] and confirmed, by the measurement of timing variation, to orbit the pulsar PSR1257+12. Although very powerful, this technique was restricted to a small number of very particular hosts. Doppler velocimetry, instead, could be applied, with good results, to almost any 'quiet' star showing a reasonable amount of narrow absorption lines in its spectrum. The continuous improvement of this technique led, in 1995, to the discovery of the first giant planet around the Sun-like star 51 Pegasi[5] and marked the start of an intensive era of discoveries (see Review by Mayor *et al.* on **page XXX**).

Since the discovery of 51 Peg b, microlensing, transit searches and direct imaging has delivered, together with Doppler velocimetry, an increasing number of planets and planetary candidates. Better instruments and improved detection limits have pushed our capabilities towards the detection of low-mass and small planets. Furthermore, the discovery of multi-planetary systems is the direct consequence of long-term, high-precision programmes. A new breakthrough was made thanks to the space-based transits searches Convection, Rotation and Planetary Transits (CoRoT)[6] and Kepler[7]. These missions have made a significant contribution to the statistical study of exoplanetary systems.

In this Review, we will discuss techniques and instruments that have contributed the most to our understanding of exoplanets. We will also provide an overview of present and future instrumentation, and describe how the field is moving from simple detection and statistical studies to the characterization of individual planets, their interior and their atmospheric composition.

Stellar radial velocities

Giant planets on short orbits induce radial-velocity variations in their host stars of several tens to a few hundreds of metres per second. Early Doppler velocimeters[8,9] delivered 200–500 m s^{-1} precision. With the use of a hydrogen-fluoride absorption cell the precision could be improved by one order of magnitude[10]. In the late 80s and early 90s an entire suite of new techniques and spectrographs[11–14] led to an improvement of the radial-velocity precision down to 3–15 m s^{-1}. This better precision led, in turn, to the discovery of 51 Peg b[5] and the era of giant-planet detection.

Would it be possible to detect terrestrial mass exoplanets by the Doppler technique? Some astronomers believed that improving the instrumental precision would be a key element[15]. Confirmation of this belief was provided by the discovery of μ Arae c in 2004 (ref. 16). At only 10 times the mass of Earth and with an orbit of 9.6 days, this planet produces a stellar radial-velocity pull of 3 m s^{-1} semi-amplitude. The detection of this tiny signal required a new generation of spectrographs, such as High Accuracy Radial Velocity Planet Searcher (HARPS)[17]. It represented the first step towards the detection and characterization of a vast population of Neptune-mass planets and super-Earths. The longer the temporal coverage and the better the instrumental precision, the smaller the radial-velocity signals (see for example the detection of α Cen B b[18]) that could be detected (Fig. 1).

The Doppler measurement consists of determining the wavelength of an identified spectral line and comparing it with the theoretical value it would have when transferred into the Solar System's rest frame. The Doppler equation links the measurement to the theoretical wavelength by the relative-velocity vector, finally delivering the projection of this vector in the direction of the line of sight (radial velocity). To increase the precision, the average, over several thousands of spectral lines, is computed. It should be noted, however, that the radial-velocity measurement is affected by several potential error sources that have been discussed extensively[10,14,19,20]. The main error sources are: photon noise[14,21]; instrumental errors[11,14,19]; spectrograph-illumination effects[22,23]; spectral contamination[19,24]; and stellar 'noise'[25–39], commonly referred to as stellar jitter. The term stellar jitter masks various stellar causes that produce radial-velocity effects at all timescales and of different magnitude. The discussion of all these effects lies beyond the scope of our Review. Nevertheless, it is important to be reminded that stellar jitter is probably the strongest limitation for Doppler velocimetry when aiming for sub-metre-per-second precision.

Present and future Doppler spectrographs need to address the mentioned limitations. As a first step, telescope size should be increased because high-spectral-resolution measurements are photon-starved, even for relatively bright targets. The gain obtained with a large telescope

[1]Observatoire Astronomique de l'Université de Genève, 51 Chemin des Maillettes, 1290 Versoix, Switzerland. [2]Swiss Federal Institute of Technology, Institute for Astronomy, Wolfgang-Pauli-Strasse 27, 8093 Zurich, Switzerland.

is, however, easily lost if spectral resolution is low. In fact, for unresolved spectral lines the measurement precision increases significantly with increasing spectral resolution[21]. In the photon-noise-limited regime the error ε_{bary} on the line-centre measurement can be estimated by:

$$\varepsilon_{bary} = \frac{\sigma^{1.5}}{\sqrt{2 \cdot I_0} \cdot EW} \cdot \sqrt{\left(1 - \frac{c}{2}\right)}$$

where σ is the measured width of the spectral line as seen through the spectrograph; $c = (I_{min} - I_0)/I_0$ is the measured line contrast; and $EW = \sigma c$ is the equivalent width. I_0 and I_{min} designate the photoelectron counts per resolution element in the continuum and the line minimum, respectively. It must be noted that the resolution element can be represented either by the detector pixel or by the wavelength unit as long as all the parameters are expressed in the same units. It is now commonly agreed that a spectral resolution of at least $R = \lambda/\Delta\lambda = 100{,}000$ should be used to guarantee the best precision on slowly rotating, quiet, solar-type stars. Spectral resolution and adequate line sampling not only allow us to achieve better signal-to-noise per spectral line, but also to reduce possible instrumental errors in both the radial-velocity measurement and the calibration process. To first order approximation, instrumental errors scale with the size of the resolution element (expressed in wavelength units). Unfortunately, with increasing telescope size, spectral resolution is a considerable driver of cost. For seeing-limited instruments the optical etendue E ($E = A \times \Omega$, the beam cross-section area times the solid angle) increases with the telescope size, and so does the instrument size if the spectral resolution is kept fixed[40]. In the era of 8-m class and extremely large telescopes (ELTs), this aspect has become a technical and managerial challenge that is nevertheless successfully addressed by employing novel optical design concepts[41–43].

All future projects for radial-velocity spectrographs (Table 1) aim to detect rocky planets in the habitable zone (the distance to the star at which liquid water can persist on the surface of the planet)[44] of a Sun-like and a low-mass star. To attain this objective they must be photon-efficient and precise to the sub-metre-per-second level. Photon efficiency is obtained with optimized designs and high-spectral resolution. High precision also requires the control of all instrumental effects. State-of-the-art instruments are therefore designed to be stable[17]. Gravity invariance and illumination stability of the spectrograph are crucial aspects that can only be obtained through a fibre feed[45–48]. Despite the intrinsic light-scrambling properties of optical fibres[49–51] it was soon realised that the illumination produced by a circular optical fibre depends on how the starlight is fed into the fibre. In other words, motions of the stellar image at the fibre entrance would produce a change in the illumination of the spectrograph and mimic a radial velocity effect. Considerable effort was invested in improving image scrambling by using double scramblers[13,49] and octagonal fibres[52,53]. Effective improvements have already been demonstrated on operational instruments[54,55].

Any instrumental effect that produces a distortion or a shift of the spectral line in the detector-pixel space will be interpreted, if not detected and recognized, as a wavelength change and thus a Doppler shift[20]. Two methods of tracking the instrumental profile changes have successfully been applied in the past. The first is to superimpose an absorption spectrum of a reference gas cell[10,14,56] on the stellar spectrum, such that the instrumental profile is continuously measured. This so-called self-calibration technique is particularly useful and effective in spectrographs with varying instrument profiles, as is the case for slit spectrographs. The disadvantages of this technique are the restricted bandwidth of the gas-cell spectrum, the loss of efficiency due to absorption in the light path, and the necessity for a sophisticated deconvolution process to recover the stellar spectrum and thus the radial velocity. This latter step requires the introduction of many additional parameters for spectral modelling. To obtain a given precision, higher signal-to-noise spectra must be acquired. The second method, the 'simultaneous reference technique'[13,17], is conceptually opposite. It assumes a stabilized instrumental profile that does not change between two wavelength calibrations of the spectrograph, such that the determined relationship between the detector pixel and the wavelength remains valid over these timescales (typically a night). A second channel carrying a spectral reference is continuously fed to the spectrograph to monitor and correct for potential instrumental drifts or instrument profile changes. It must be guaranteed, however, that the changes that the scientific and the reference channels are subject to are identical over the timescale of one observing night. Therefore, the whole design of the instrument must be optimized for stability of the instrumental profile, requesting fibre feed and light scrambling, as well as pressure, mechanical, thermal and optical stability. The effort is compensated for by an unrestricted spectral bandwidth and the acquisition of an 'uncontaminated' scientific spectrum.

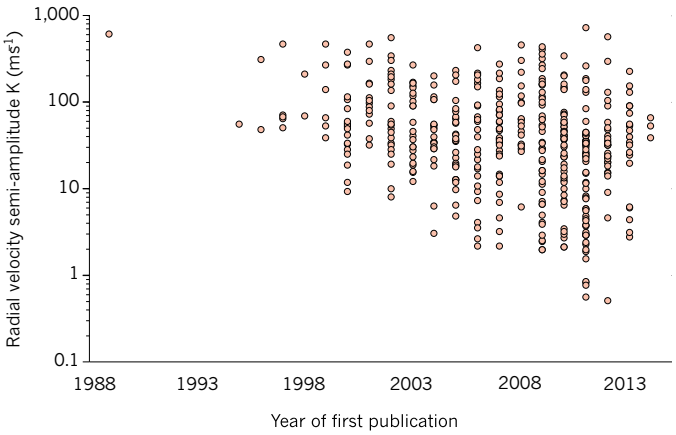

Figure 1 | Radial-velocity semi-amplitude of planetary-mass companions. All planets discovered by the Doppler technique from 1989 to present day are plotted. Remarkably, the detection limit improved by three orders of magnitudes in less than three decades. The underlying data were retrieved from http://www.exoplanets.org.

Although, in the case of the self-calibration technique, the instrument profile is supposed to be recoverable by deconvolution, there seems to be general agreement that low-order instrument-profile changes must, in any case, be avoided and that a stable instrument will eventually deliver more precise measurements. There is also agreement that better calibration sources are needed. The laser-frequency comb[57–62], when available at full potential, will provide the required calibration accuracy and precision. In the meantime, alternative sources are being developed, for example, passive Fabry–Pérot cavities[63–65] for simultaneous reference, or actively stabilized Fabry–Pérot systems for wavelength calibration[66].

The near-infrared wavelength region is becoming increasingly interesting for two other reasons. First, M dwarfs are much brighter in the infrared than in the visible[67]. These stars are cooler and thus their habitable zone lies closer to the host star. In addition the parent star is less massive. Potential habitable planets are, therefore, more easily detected by radial velocity[67]. Second, the influence of spots is strongly reduced in the near-infrared compared with the visible[68–70]. Furthermore, a comparison with radial-velocity determined in the visible wavelength range might help to discriminate a planet-induced velocity change from a stellar effect. For these reasons, many new instruments[71–76] (Table 1) will operate in the infrared wavelength domain. The use of adaptive optics[77] could be a means of reducing the size and cost of these instruments.

Transit photometry and spectroscopy

There are two approaches to detecting planetary transits: surveying as many stars as possible with one or several photometers in the hope of detecting new exoplanets through their transits, and photometrically following up planets discovered by Doppler velocimetry around their predicted inferior conjunction time. (The inferior conjunction denotes the orbital configuration where the planet lies between its host star and the observer; a transit occurs at the inferior conjunction if the orbital plane of the planet is aligned with the line of sight.) In the first method, the expected depth of the transit light curve dictates the photometric

Table 1 | Non-exhaustive table of present (active) and future (approved) high-precision Doppler velocimeters

Instrument/technique	Telescope/observatory	Start of operations	Band (μm)	Spectral resolution	Efficiency (%)	Precision (m s^{-1})
Hamilton[180]/self-calibration	Shane 3 m/Lick	1986	0.34–1.1	30,000–60,000	3–6	3
UCLES[181]/self-calibration	3.9-m AAT/AAO	1988	0.47–0.88	~100,000	NA	3–6
HIRES[12]/self-calibration	Keck I/Mauna Kea	1993	0.3–1.0	25,000–85,000	6	1–2
CORALIE[13]/sim. reference	EULER/ESO La Silla	1998	0.38–0.69	60,000	5	3–6
UVES[182]/self-calibration	UT2–VLT/ESO Paranal	1999	0.3–1.1	30,000–110,000	4–15	2–2.5
HRS[183]/self-calibration	HET/McDonald	2000	0.42–1.1	15,000–120,000	6–9	3–6
HDS[184]/self-calibration	Subaru/Mauna Kea	2001	0.3–1.0	90,000–160,000	6–13	5–6
HARPS[18]/sim. reference	3.6 m/ESO La Silla	2003	0.38–0.69	115,000	6	< 0.8
FEROS-II[185]/sim. reference	2.2 m/ESO La Silla	2003	0.36–0.92	48,000	20	10–15
MIKE[186]/self-calibration	Magellan II/Las Campanas	2003	0.32–1.00	65,000–83,000 and 22,000–28,000	20–40	5
SOPHIE[187]/sim. reference	1.93 m/OHP	2006	0.38–0.69	39,000 and 75,000	4 and 8	2
CRIRES[188]/self-calibration	UT1–VLT/ESO Paranal	2007	0.95–5.2	~100,000	15	5
PFS[189]/self-calibration	Magellan II/Las Campanas	2010	0.39–0.67	38,000–190,000	10	1
PARAS[190]/sim. reference	1.2 m/Mt. Abu	2010	0.37–0.86	63,000	NA	3–5
CAFE[191]/sim. reference	2.2 m/Calar Alto	2011	0.39–0.95	~67,000	25	20
CHIRON[192]/self-calibration	1.5 m/CTIO	2011	0.41–87	80,000	15	<1
HARPS-N[54]/sim. reference	TNG/ORM	2012	0.38–0.69	115,000	8	<1
LEVY[193]/self-calibration	APF/Lick	2013	0.37–0.97	114,000–150,000	10–15	<1
EXPERT-III[194]/NA	2-m AST/Fairborn	2013	0.39–0.9*	100,000*	NA	NA
GIANO[71]/self-calibration	TNG/ORM	2014	0.95–2.5	50,000	20	NA
SALT–HRS[195]/self-calibration	SALT/SAAO	2014	0.38–0.89*	16,000–67,000*	10–15*	3–4*
FIRST[194]/NA	2-m AST/Fairborn	2014	0.8–1.8*	60,000–72,000*	NA	NA
IRD[73]/sim. reference	Subaru/Mauna Kea	2014	0.98–1.75*	70,000*	NA	1*
NRES/NA	6 × 1-m/LCOGT	2015	0.39–0.86*	53,000*	NA	3*
MINERVA/self-calibration	4 × 1-m/Mt. Hopkins	2015	0.39–0.86*	NA (Kiwispec)*	NA	1*
CARMENES[72]/sim. reference	Zeiss 3.5-m/Calar Alto	2015	0.55–1.7*	82,000*	10–13*	1*
PEPSI[196]/sim. reference	LBT/Mt. Graham	NA	0.38–0.91*	120,000–320,000*	10*	NA
HPF[74]/sim. reference	HET/McDonald	NA	0.98–1.40*	50,000*	4*	1–3*
CRIRES+/self-calibration	VLT/ESO Paranal	2017	0.95–5.2*	~100,000*	15*	<5*
ESPRESSO[42]/sim. reference	All UTs–VLT/ESO Paranal	2017	0.38–0.78*	60,000–200,000*	6–11*	0.1*
SPIROU[76]/sim. reference	CFHT/Mauna Kea	2017	0.98–2.35*	70,000*	10*	1*
G-CLEF[43]/sim. reference	GMT/Las Campanas	2019	0.35–0.95*	120,000*	20*	0.1*

For the spectral band and the spectral resolution the maximum value is given. The total efficiency has been extrapolated to include slit losses, and telescope and atmospheric throughput. The radial-velocity precision was estimated from published orbits or standard star's velocities. Historical instruments have not been listed. It is interesting to note that most of the planets discovered between 1995 and 2003 were detected using a small number of precision instruments: HIRES (High Resolution Echelle Spectrometer) at the 10-m Keck i telescope in Hawaii, CORALIE at the European Southern Observatory (ESO) 3.6-m telescope in La Silla, The Hamilton Spectrograph at the Shane 120-inch telescope at Lick, ELODIE at the 1.93-m telescope of the Haute-Provence Observatory[13], AFOE (Advanced Fiber-Optic Echelle) on the 1.5-m telescope at the Whipple Observatory[197], UCLES (University College London Échelle Spectrograph) at the Anglo-Australian Telescope (AAT), Coudé Echelle Spectrograph[198] on the 2.7-m telescope, the Sandiford Cassegrain Echelle spectrograph[198] on the 2.1-m telescope and the High-Resolution Spectrograph (HRS) at the Hobby-Eberly Telescope (HET), all of them at the McDonald Observatory. After 2003 the HARPS spectrograph opened a new window on the domain of super-Earths and mini-Neptunes by improving the radial-velocity precision below the metre-per-second level. Since then, the metre-per-second precision has become a 'standard' and a goal for most of the Doppler-velocimeter projects presented in the Table. AAO, Australian Astronomical Observatory; APF, Automated Planet Finder; AST, Automatic Spectroscopic Telescope; CAFE, Calar Alto Fiber-fed Echelle; CARMENES, Calar Alto High-Resolution Search for M dwarfs with Exo-Earths with Near-Infrared and Optical Echelle Spectrographs; CFHT, Canada-France-Hawaii Telescope; CTIO, Cerro Tololo Inter-American Observatory; ESPRESSO, Echelle Spectrograph for Rocky Exoplanet and Stable Spectroscopic Observations; EXPERT-III, Extremely High Precision Extrasolar Planet Tracker III; FEROS-II, Fiberfed Extended Range Optical Spectrograph; FIRST, Florida infrared Silicon Immersion Grating Spectrometer; G-CLEF, GMT-CfA Carnegie, Catolica, Chicago Large Earth Finder; GMT, Giant Magellan Telescope; HPF, Habitable-zone Planet Finder; HDS, High Dispersion Spectrograph; IRD, Infrared Doppler; LBT, Large Binocular Telescope; LCOGT, Las Cumbres Observatory Global Telescope Network; MINERVA, Miniature Exoplanet Radial Velocity Array; MIKE, Magellan Inamori Kyocera Echelle; NRES, Network of Robotic Echelle Spectrographs; OHP, Observatoire de Haute Provence; ORM, Observatorio del Roque de los Muchachos; PARAS, PRL Advanced Radial-velocity All-sky Search; PEPSI, Potsdam Echelle Polarimetric and Spectroscopic Instrument; PFS, Planet Finder Spectrograph; SAAO, South African Astronomical Observatory; SALT, Southern African Large Telescope; SOPHIE, Spectrographe pour l'Observation des Phénomènes des Intérieurs Stellaires et des Exoplanètes; SPIROU, SpectroPolarimètre Infra-Rouge; TNG, Telescopio Nazionale Galileo; UT, Unit Telescopes; UT2–VLT, Unit Telescope 2–Very Large Telescope; UVES, Ultraviolet and Visual Echelle Spectrograph. NA, not available or non-reliable information; sim. reference, simultaneous reference technique.
*Indicates design values.

precision needed — for Jupiter-sized planets in transit across Sun-like stars the transits can be detected from the ground with amateur telescopes. Hot Jupiters, however, are only found orbiting about 1% of nearby solar-type stars[78], requiring observers to maximize the number of surveyed stars. Bright main sequence stars can be surveyed over a large fraction of the sky by wide-field cameras with small aperture telescopes and charge-coupled devices (CCDs), as illustrated by the Wide Angular Search for Planets[79] (WASP). Observations from a single location are limited, however, by the duration of the night. Time and sky coverage can be further improved with networks of small telescopes that relay from different longitudes, such as the Hungarian Automated Telescope Network[80] (HATNet) or the Trans-Atlantic Exoplanet Survey[81] (TrES).

The other strategy is to stare at crowded stellar fields. The 1.3-m telescope of the Optical Gravitational Lensing Experiment (OGLE) yielded the first discoveries of exoplanets through the transit method[82] by applying this strategy. The confirmation of these detections with velocimetry[83], however, required a large observational effort because of the faint optical magnitudes (denoted V) of the stars surveyed (V = 14–16 mag). The

first space missions dedicated to the search for transiting exoplanets, CoRoT[6,84] and Kepler[7], also stared at dense fields with high-cadence precise (relative) photometry (see the Reviews by Hatzes on **page XXX** and Lissauer *et al.* on **page XXX**). Together, these satellites have surveyed several hundred thousand stars. Radial-velocity follow-up of CoRoT and Kepler exoplanet candidates remains difficult owing to the faint magnitudes of the host stars and the large number of targets needing follow-up. The faintness of the host stars also sets severe limits on the use of photon-starved techniques, such as transmission spectroscopy for the study of the planetary atmospheres. This technique requires bright host stars (Fig. 2), such as the hosts of planets discovered through velocimetry and later detected in transit. Only nine such exoplanets are known so far, but future space missions will search for more of these planets. In the meantime, and from the ground, planets transiting small stars such as M dwarfs are being looked for, because the transit signal is inversely proportional to the square of the stellar radius. The MEarth survey[85], composed of eight identical robotically controlled 40-cm telescopes with CCD detectors, found a super-Earth[86] that is especially amenable to follow-up atmospheric studies[87–91].

Studies of exoplanetary atmospheres

The hot gas giant HD 209458b was the first exoplanet captured in transit by two separate small telescopes[92,93], with a relative photometric precision of 0.2–0.4%. This transit was also the first exoplanet-related event observed from space: the 2.4-m Hubble Space Telescope measured the transit light curve to a precision of 110 p.p.m. per minute of observation[94]. The photometric observations of HD 209458b were obtained by integrating the stellar spectra collected before, during and after the transit by the Space Telescope Imaging Spectrograph (STIS)[95] CCD detector. These spectra were recorded with a medium-resolution (R = 5,540) grism of medium band pass, notably including the sodium doublet at 589 nm. The first transmission signature of an exoplanetary atmosphere was reconstructed from this data set by measuring, during the transit, an extra absorption of 200 p.p.m. in the sodium lines[96]. The far-ultraviolet channel of the STIS instrument, which collects ultraviolet photons with a multi-anode microchannel array (MAMA) detector, was used to observe the transit of HD 209458b over the stellar Lyman-α emission of atomic hydrogen at 121 nm. These measurements led to the discovery of an extended upper atmosphere to the planet[97].

HD 209458b remained, for quite some time, the only known transiting exoplanet. By the time additional transiting exoplanets were announced (in 2004), STIS had experienced a power-supply failure. The instrument was only repaired in 2009 during the last servicing mission of Hubble. Arguably, the main effect of the STIS failure was to shift the field of exoplanetary atmospheres into the infrared. After 2004, and despite successful attempts to record precise transit light curves with the Advanced Camera for Surveys on board Hubble[98], the 85-cm Spitzer Space Telescope became the prime observatory not only for transits, but also for eclipses of planets by their stars, which can occur at superior conjunctions (the orbital configuration opposite the inferior conjunction, when the planet passes behind the star). Broadband photometry of these eclipses with the Infrared Array Camera (IRAC)[99] on Spitzer revealed the thermal emission from exoplanets, the first example of direct detection of light from a planet orbiting a star[100–102]. The instrument has four broadband infrared channels collecting light on two detectors made of indium antimonide (3.6 μm and 4.5 μm channels) and arsenic-doped silicon (5.8 μm and 8.0 μm channels).

The first infrared observation of a planetary transit[103] was obtained with the Multiband Imaging Photometer for Spitzer (MIPS) at 24 μm. These observations were limited by the low stellar flux in the mid-infrared. Furthermore, transit observations in the near infrared exhibited large instrumental effects, precluding the detection of molecular signatures. Both photometry with IRAC[104–106] and spectroscopy with the Near-Infrared Camera and Multi-Object Spectrometer (NICMOS)[107] on Hubble yielded non-reproducible results or were of insufficient quality for unambiguous interpretation[108–110]. Eclipse spectroscopy of the dayside

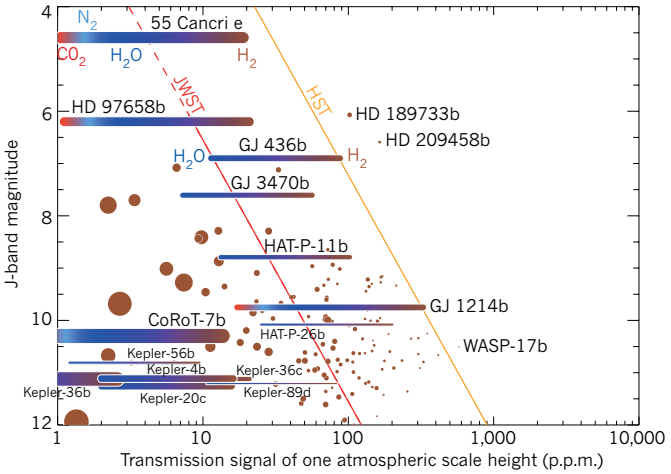

Figure 2 | Detectability of planetary atmospheres. The signal of one atmospheric scale height seen in transmission during transit is plotted against the stellar J magnitude. The signal is calculated in parts per million (p.p.m.) as $2 \times 10^6 (\Delta F/F)(H/R_p)$, where $\Delta F/F$ is the transit depth and H is the atmospheric scale height. This quantity scales here with the equilibrium temperature of the planet and is inversely proportional to the acceleration of gravity at the surface of the planet and the mean molar mass (μ) of the atmosphere. The atmospheric signal is proportional to the planet mean density. The size of the circles (and the thickness of the colour bars) scales with the density to show this effect. For giant exoplanets (brown circles), the atmosphere is assumed to be primarily composed of molecular hydrogen (H_2) and helium (μ = 2.3 g mol^{-1}). For lower-mass planets, such as Neptunes ($10 < M_p < 60\ M_E$, where M_E is the mass of Earth and M_p is the mass of the planet) and super-Earths ($M_p < 10\ M_E$), the atmospheric composition is unknown and the colour bar extents represent all possible signal values assuming hydrogen and helium (μ = 2.3 g mol^{-1}, brown) and water (H_2O, μ = 18 g mol^{-1}, blue) dominated atmospheres for Neptunes, and molecular nitrogen (N_2, μ = 28 g mol^{-1}, light blue), and carbon dioxide (CO_2, μ = 44 g mol^{-1}, red) dominated atmospheres for super-Earths, in addition to the two earlier types. Approximate Hubble Space Telescope (HST) and JWST 3-σ detection limits (orange and red lines, respectively) are shown. Only super-Earths and Neptunes with a mass determined to better than 20% are represented.

emission of HD 189733b obtained with the third instrument on Spitzer, the Infrared Spectrograph (IRS)[111] providing low-resolution (R = 80) and spectral coverage from 5 μm to 14 μm, also had to be corrected for instrumental effects[112]. The IRS data nonetheless provided evidence for molecular absorption in an exoplanet atmosphere[113]. Unfortunately, the use of IRS was terminated after Spitzer ran out of cryogen in May 2009. Meanwhile, Spitzer continues observing with IRAC 3.6-μm and 4.5-μm channels, now commonly used to obtain precise transit light curves of exoplanets down to the super-Earth size regime[114,115].

Ground-based atmospheric characterization of exoplanets advanced through the use of high-resolution spectrographs. The signature of sodium in the atmosphere of HD 209458b was found[116] in data taken with the High Dispersion Spectrograph (R = 45,000) at the Subaru 8-m telescope[117]. The technique, differential spectroscopy, involves calibrating the signal in the spectroscopic features with the continuum signal in the vicinity of the features. The 'absolute' transit depth is lost, but the transmission signal can be retrieved, assuming that telluric absorption can be sufficiently calibrated. Another method is to calibrate the wavelength-dependent signal using other stars within the field of view of the instrument. This can be achieved in spectrophotometry for systems with nearby reference stars[118,119] or in spectroscopy with slit masks positioned on the target and on several reference stars in the field[87]. A breakthrough was made possible by the Cryogenic High-Resolution Infrared Echelle Spectrograph (CRIRES) on the Very Large Telescope (VLT). Its high resolution (R = 100,000), although over a narrow (50 nm) wavelength infrared region, allows tracking of the wavelength shift of individual spectral features composing molecular bands of water, carbon monoxide or carbon

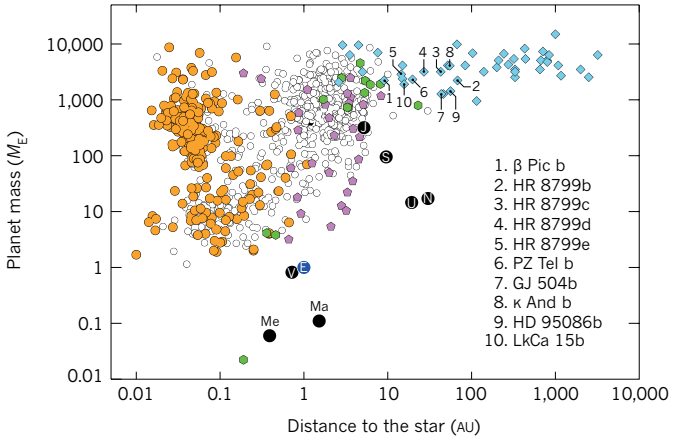

Figure 3 | Mass and semi-major axis of known planets. Planetary mass is plotted as a function of the semi-major axis (the distance to the host star). Solar-system planets are shown by black circles (Me, Mercury; V, Venus; Ma, Mars; J, Jupiter; S, Saturn; U, Uranus; N, Neptune) and Earth (E) is in blue. Exoplanets detected with different techniques and instrumentation are shown. Doppler velocimetry (white), transit with a measured mass (orange), direct imaging (blue), microlensing (pink), and pulsation timing (green). Among the direct-imaging planets, only ten (labelled) were found within 100 AU of their host and a mass ratio between the companion and its host star $q < 0.02$. Data underlying this plot were retrieved from the Exoplanet Encyclopaedia[199].

dioxide that are present in the atmosphere of the planet as the planet orbits the star[120–122]. The method works for transiting and non-transiting planets alike, giving access to the brightest exoplanetary systems, such as that of τ Boötis[123]. Its application to the directly imaged planet β Pictoris b[124] led to the determination of the spin velocity of the planet[125].

The refurbishment of Hubble in May 2009 enabled the recovery of STIS capabilities and the start of operations of both the Cosmic Origins Spectrograph[126] (COS) in the far-ultraviolet and the Wide-Field Camera-3 (WFC3)[127] in the near-infrared. COS and STIS provided observations and confirmation of the atmospheric mass loss from HD 209458b in the singly ionized carbon lines at 133 nm[128]. These measurements were extended to other exoplanets[129–133]. Visible STIS spectra revealed atomic signatures and the presence of light scattering processes in the upper atmospheric layers of HD 189733b[129,134], and observations of the eclipse of HD 189733b with a low-resolution grating from 290 nm to 570 nm also yielded the first chromatic measurements of a planetary albedo[135]. The WFC3 infrared channel was successfully used for slitless grism spectroscopy of exoplanetary transits in the near-infrared, achieving near-photon-noise transmission spectroscopy of super-Earths, Neptunes and gas giants between 1.1 μm and 1.7 μm[90,136–143], and detecting the 1.38-μm water band in some of these planets.

Direct imaging and astrometry

Despite many years of technological development, the search for ideal targets, improved analysis algorithms and investment in observing time on leading telescopes, it was not until 2008 that the first direct images of an exoplanetary system around a star were obtained. The multi-planet system HR 8799, with all planets[144] orbiting the intermediate mass host star in the same rotation sense, was a remarkable (and a lucky) breakthrough. Interpretation of the contemporaneous discovery of a faint point source around the debris disk host star Fomalhaut[145] has turned out to be more complex than anticipated[146]. Finally, at the end of 2008, a giant planet was found around β Pic[124,147–149] within the prototypical debris disk first imaged in the early 1980s[150]. These discoveries were preceded by several others (some of which were spurious), often around very young objects still in the process of becoming a star. For example, the companion to 2MASSWJ 1207334-393254 (a very young brown dwarf) was discovered[151] through adaptive-optics-assisted near-infrared imaging with the NACO instrument on the VLT. This discovery was notable because the system is very young, making detection of a self-luminous planetary mass object easier; the central host object is of very low mass and thus of modest luminosity relative to the planetary mass companion; and NACO is equipped with an infrared wave-front sensor, which is important to allow observations of this class of cool primaries. However, the mass ratio (q) of the brown dwarf to the companion is consistent with many examples of binary star systems of higher mass. So far, there have been 10 objects found within 100 AU of their host with a mass ratio between the companion and the host star of $q < 0.02$ (Fig. 3; http://exoplanet.eu/). These restrictions suggest that they may have formed like planets in our Solar System, but this is not at all certain. There are dozens of objects that have larger mass ratios (particularly around very low-mass primaries), as well as objects with low-mass ratios, but found at larger radii (out to more than 1,000 AU). One major caveat to these studies is that the masses are inferred from theoretical models[152] based on the shape of the spectral energy distribution and luminosity, as well as knowledge about the central star (primarily age, but also composition).

State-of-the-art instruments require advanced adaptive optics to correct for the blurring effects of Earth's atmosphere[153]. Although the diffraction limit improves at shorter wavelengths, high performance adaptive optics are more challenging, leading to compromises for instrument design between 0.5–5.0 μm. Even at the diffraction limit of an 8-m class telescope, it is only possible to reach orbital separations of 3 AU at 1.65-μm wavelength for stars out to a 50 pc distance. The younger a planet is, the hotter and brighter it is, making its detection and characterization easier. Nearby stars tend to be old (1–3 gigayear) and the youngest objects, which are more rare, are located at greater distances. Thus, another compromise needs to be found between available target sample and ease of detection, which translates directly into a balance between detectable mass (better for younger, more distant objects) and orbital separation (better for nearby stars). Results so far suggest that massive gas-giant planets ($> 2\ M_J$) are rare at large orbital radii[154] (for example, beyond 50 AU). However, new instruments utilizing extreme adaptive optics (resulting in an increase of hundreds to thousands of actuators controlling the shape of the deformable mirror, for example, the Spectro-Polarimetric High-Contrast Exoplanet Research (SPHERE)[155] instrument and the Gemini Planet Imager (GPI)[156])will improve the inner working angle that can be reached at all wavelengths of operation, although in particular it will open up the possibility of Strehl ratios above 30% in the red visible[157]. It is also worth mentioning that great improvements in data acquisition modes and analysis software (differential imaging through angular, polarimetric and spectral difference) have greatly enhanced planet-detection capabilities[158–162]. In addition, the development of diffraction-suppression optics continues — as observations are contrast-limited close to the star. In the photon-noise limit, which is not often reached even around early type bright stars, sparse aperture masking[163] and coronography can improve the achievable contrast limit using techniques such as apodizing phase plates[164], vector vortex[165], phase-induced amplitude apodization[166] and classical Lyot coronography[167]. Marked improvements in diffraction suppression, stability and quality of adaptive optics, as well as in post-processing algorithms, are needed to reach the fundamental background-limited sensitivity close to the diffraction limit. The inner working angle, at which the background limit is reached, is 10 times larger than the diffraction limit. The implementation of low-noise infrared wave-front sensors is another key area of development, particularly in their application to imaging surveys of fainter lower-mass stars and brown dwarfs. Building the observational data to constrain the frequency of planets as a function of planet mass, orbital separation and primary-star mass will provide powerful tests for theories of planet formation.

The James Webb Space Telescope (JWST) will launch in 2018 and will provide powerful capabilities for direct imaging, including coronagraphy. All of its instruments will make great contributions to finding and characterizing exoplanets resolved from their host stars, including some of those already known today. In particular, its short-wavelength imager, Near Infrared Camera (NIRCam), will be able to detect planets below the mass of Saturn beyond 30 AU around close-by stars. The

Near-Infrared Imager and Slitless Spectrograph (NIRISS) will utilize a sparse aperture mask to detect bright companions below the diffraction limit at 1–2.3 μm wavelength. It will be particularly useful for surveys of very young stars for which planetary companions will be brightest relative to the central star. The Mid-Infrared Instrument (MIRI), the long-wavelength camera/spectrograph on JWST, will provide additional characterization of planetary atmospheres from 5 μm to 28 μm, and the Near-Infrared Spectrograph (NIRSpec, 1–5 μm) will be equipped with an integral field spectrograph that is capable of providing high-quality spectra of close companions.

Although JWST will be the most powerful telescope ever in terms of infrared sensitivity, it will not provide enhanced spatial resolution compared with the current generation of 6–10-m telescopes and will not provide unique capabilities for high-contrast imaging at inner working angles below 0.1 arcsec. Because we know that the distribution of giant gaseous planets rises with orbital radius out to 3 AU, and because massive gas giants are rare beyond 30 AU, it is likely that most Jupiter-mass planets will be found at intermediate separations. The next generation of ELTs will enable us to cross the 10 AU threshold in angular resolution of accessible targets, pushing the detectable separation down to 3 AU and enabling vast synergies between Doppler velocimetry and astrometry. The Large Binocular Telescope Interferometer (LBTI) is the first optical telescope with an effective resolution of a 22.8-m baseline[168], although it is not a filled aperture, thus limiting its sensitivity. The European ELT (E-ELT), with its aperture of 39 m, will integrate a suite of imaging and spectroscopic instruments (HARMONI, MICADO, METIS and eventually EPICS) to enable efficient imaging of exoplanets at diffraction-limited inner working angles below 0.1 arcsec. Similar instruments are planned for the two other ELT projects — the Thirty Meter Telescope (TMT) and the Giant Magellan Telescope (GMT). Considerable thought is being devoted to working out how to reach the fundamental background limit when approaching the diffraction limit, which, along with sensitivity and spatial resolution of these ELTs, would represent a major breakthrough. The removal of so-called quasi-static speckles is the key; this can be achieved, in principle, through sophisticated calibration schemes for adaptive-optics systems to enable the commanded removal of speckles, or equally by sophisticated analysis of the wavefront sensor camera data and telemetry to analyse residual errors in post-processing[169]. In predicting the performance of these future telescopes some take a conservative approach, whereas others believe they could reach the ultimate limit. Either way, these ELTs will represent a huge breakthrough in the capacity to directly image planets around nearby stars. If the technological challenges are mastered, the E-ELT will have a reasonable chance of obtaining a direct image of a super-Earth within 1 AU of the nearest stars[170].

In late 2013, the European Space Agency launched Gaia, which has the ability to reach micro-arcsecond astrometric precision. Owing to better performances, this mission will allow the exploration of a wider parameter space to detect motions in the plane of the sky due to the orbit of the host star and planet around a common centre of mass. As the precision will fall for fainter stars, Gaia will be sensitive to the lowest-mass planets only around stars in the solar neighbourhood, but will detect hundreds — if not thousands — of gas-giant planets within hundreds of parsecs[171]. Furthermore, this will open up the synergistic possibility to directly image some of these objects, providing ground-truth for models of their evolution. Ground-based astrometry will also play a part, as could JWST and other facilities. For instance, ground-based direct imaging could deliver astrometric measurements at 100 micro-arcsecond precision[172].

A bright and multi-technique future

In the past, our focus was on discovering new exoplanets and acquiring statistics about their diversity, which, in turn, concerned mainly external (orbital) parameters (Fig. 3). Now, interest is moving towards the detailed characterization of specific planets and planetary systems. Orbital parameters, host-star characteristics, synchronization and planetary spin, irradiation, planet density and internal structure, atmospheric composition, and physical conditions must be characterized in order for us to understand the formation processes and the observed diversity.

Increasing the number of targets amenable to further characterization is the prime goal of several dedicated space mission projects: the extension of the Kepler mission (K2)[173], NASA's Transiting Exoplanet Survey Satellite (TESS)[174] and ESA's Planetary Transits and Oscillations of Stars mission (PLATO)[175] will obtain photometric measurements of bright stars located almost everywhere in the sky, and thus find many new transiting planets around bright stars. These space missions will be complemented by new ground-based surveys dedicated to the search for transits across different types of stars, for example, the Next Generation Transit Survey (NGTS), the Search for Habitable Planets Eclipsing Ultra-cool Stars (SPECULOOS), the Exoplanets in Transit and Their Atmosphere (ExTrA) and the Multi-Site All-Sky Camera (MASCARA)[176].

The planets transiting bright stars will enable follow-up observations and characterization of the planets by other techniques. The Swiss-ESA spacecraft CHEOPS (Characterising Exoplanets Satellite)[177,178] will, by transit photometry, measure precise radii and bulk densities of known exoplanets and select the best-suited targets for atmospheric characterization by future spectrographs from space or on large ground-based telescopes. JWST will have unprecedented thermal infrared sensitivity. Its four instruments will, in addition to the direct imaging of planets, attempt transit observations at low-to-medium-resolution (R = 100–1,500) in the near- and mid-infrared domain for atmospheric characterization. Whereas several of the known hot gas giants will be amenable to detailed studies with JWST (Fig. 2), additional low-mass targets, Neptunes, super-Earths and Earth-like planets, will be delivered by TESS, CHEOPS and PLATO.

Atmospheric characterization of transiting and non-transiting exoplanets has already been initiated with current ground-based direct imaging and resolved spectroscopy as well as high-resolution spectrographs (for example, CRIRES and HARPS). These capabilities will be considerably extended with the upcoming generation of visible and near-infrared instruments equipping 4-m to 8-m telescopes. The advent of ELTs such as E-ELT, TMT and GMT, in combination with high spatial and spectral resolution, will amplify this tendency and open up a new parameter space, for instance by enabling the detection of bands of molecular oxygen on super-Earths transiting M dwarfs[179].

Techniques such as radial-velocity, photometry, astrometry, imaging and spectroscopy will all contribute to the field of exoplanets. Whereas in the past the groups using these techniques seemed to be in competition, now, in view of achieving a comprehensive understanding of the 'new worlds' we are looking for, the results they produce are highly complementary. The more mature the field becomes, the more we understand that we will not find another Earth with one single mission, but only with the combination of all the tools that are offered to us over the next decades. ■

Received 26 May; accepted 15 July 2014.

1. Van de Kamp, P. Parallax, proper motion, acceleration, and orbital motion of Barnard's star. *Astron. J.* **74,** 238 (1969).
2. McCarthy, D. W. J. & Probst, R. G. Detection of an infrared source near VB 8: the first extra-solar planet? *Bull. Am. Astron. Soc.* **16,** 965 (1984).
3. Latham, D. W., Stefanik, R. P., Mazeh, T., Mayor, M. & Burki, G. The unseen companion of HD114762 — a probable brown dwarf. *Nature* **339,** 38–40 (1989).
4. Wolszczan, A. & Frail, D. A. A planetary system around the millisecond pulsar PSR1257 + 12. *Nature* **355,** 145–147 (1992).
5. Mayor, M. & Queloz, D. A Jupiter-mass companion to a solar-type star. *Nature* **378,** 355–359 (1995).
   This article reports the discovery of the first giant planet around a Sun-like star.
6. Barge, P. *et al.* in *The CoRoT Mission, Pre-Launch Status, Stellar Seismology and Planet Finding* (eds M. Fridlund *et al.*) (ESA, 2006).
7. Borucki, W. *et al.* KEPLER: search for Earth-size planets in the habitable zone. in *Proc. IAU Symposium No. IAU253* (eds F. Pont, D. Sasselov & M. Holman) 289–299 (2009).
8. Griffin, R. F. A photoelectric radial-velocity spectrometer. *Astrophys. J.* **148,** 465 (1967).
9. Baranne, A., Mayor, M. & Poncet, J. L. Coravel — a new tool for radial velocity measurements. *Vistas Astron.* **23,** 279–316 (1979).

10. Campbell, B. & Walker, G. A. H. Precision radial velocities with an absorption cell. *Publ. Astron. Soc. Pacif.* **91,** 540–545 (1979).
This paper describes the use of absorption cells to perform high-precision Doppler measurement.
11. Walker, G. A. H. in *Complementary Approaches to Double and Multiple Star Research* (eds H. A. McAlister & W. I. Hartkopf) 67 (ASP, 1992).
12. Vogt, S. S. *et al.* HIRES: the high-resolution echelle spectrometer on the Keck 10-m Telescope. *Proc. SPIE* **2198,** 362 (1994).
13. Baranne, A. *et al*. ELODIE: A spectrograph for accurate radial velocity measurements. *Astron. Astrophys. Suppl. Ser.* **119,** 373–390 (1996).
14. Butler, R. P. *et al*. Attaining Doppler precision of 3 m s^{-1}. *Publ. Astron. Soc. Pacif.* **108,** 500 (1996).
15. Mayor, M. & Udry, S. Mass function and distributions of the orbital elements of substellar companions. *ASP Conf. Ser.* **219,** 441 (2000).
16. Santos, N. C. *et al*. The HARPS survey for southern extra-solar planets II. A 14 Earth-masses exoplanet around μ Arae. *Astron. Astrophys.* **426,** L19–L23 (2004).
The discovery of the first sub-Neptune-mass planet is reported in this paper.
17. Mayor, M. *et al*. Setting new standards with HARPS. *Messenger* **114,** 20–24 (2003).
18. Dumusque, X. *et al*. An Earth-mass planet orbiting α Centauri B. *Nature* **491,** 207–211 (2012).
This article describes the detection of the lowest-ever measure radial-velocity signal induced by a planetary companion.
19. Pepe, F. A. & Lovis, C. From HARPS to CODEX: exploring the limits of Doppler measurements. *Phys. Scr.* **130,** 014007 (2008).
This paper gives an overview of the limiting factors of Doppler velocimetry and how they may be overcome.
20. Lovis, C., Mayor, M., Pepe, F., Queloz, D. & Udry, S. Pushing down the limits of RV precision with HARPS. *Astron. Soc. Pacif. Conf. Ser.* **398,** 455 (2008).
21. Bouchy, F., Pepe, F. & Queloz, D. Fundamental photon noise limit to radial velocity measurements. *Astron. Astrophys.* **374,** 733–739 (2001).
22. Perruchot, S. *et al*. Higher-precision radial velocity measurements with the SOPHIE spectrograph using octagonal-section fibers. *Proc. SPIE* **8151,** 815115 (2011).
23. Chazelas, B. Study of optical fiber scrambling to improve radial velocity measurements: simulations and experiments. Available at http://exoplanets.astro.psu.edu/workshop/program.html (2010).
24. Pepe, F., Mayor, M., Queloz, D. & Udry, S. Towards 1 ms-1 RV accuracy. *Proc. IAU Symp.* **202,** 103 (2004).
25. Saar, S. H. & Fischer, D. Correcting radial velocities for long-term magnetic activity variations. *Astrophys. J.* **534,** L105–L108 (2000).
26. Santos, N. C. *et al*. The CORALIE survey for Southern extra-solar planets. IV. Intrinsic stellar limitations to planet searches with radial-velocity techniques. *Astron. Astrophys.* **361,** 265–272 (2000).
27. Narayan, R., Cumming, A. & Lin, D. N. C. Radial velocity detectability of low-mass extrasolar planets in close orbits. *Astrophys. J.* **620,** 1002–1009 (2005).
28. Wright, J. T. Radial velocity jitter in stars from the California and Carnegie planet search at Keck observatory. *Publ. Astron. Soc. Pacif.* **117,** 657–664 (2005).
29. Reiners, A. Activity-induced radial velocity jitter in a flaring M dwarf. *Astron. Astrophys.* **498,** 853–861 (2009).
30. Lagrange, A. M., Meunier, N., Desort, M. & Malbet, F. Using the Sun to estimate Earth-like planets detection capabilities. III. Impact of spots and plages on astrometric detection. *Astron. Astrophys.* **528,** L9 (2011).
31. Martínez-Arnáiz, R., Maldonado, J., Montes, D., Eiroa, C. & Montesinos, B. Chromospheric activity and rotation of FGK stars in the solar vicinity. An estimation of the radial velocity jitter. *Astron. Astrophys.* **520,** A79 (2010).
32. Boisse, I. *et al*. Disentangling between stellar activity and planetary signals. *Astron. Astrophys.* **528,** A4 (2011).
33. Dumusque, X., Santos, N. C., Udry, S., Lovis, C. & Bonfils, X. Stellar noise and planet detection. *Proc. 276th IAU Symposium* 527–529 (2011).
34. Dumusque, X., Lovis, C., Udry, S. & Santos, N. C. Stellar noise and planet detection. II. Radial-velocity noise induced by magnetic cycles. *Proc. 276th IAU Symposium* 530–532 (2011).
35. Cegla, H. M. *et al*. Stellar jitter from variable gravitational redshift: implications for radial velocity confirmation of habitable exoplanets. *Mon. Not. R. Astron. Soc.* **421,** L54–L58 (2012).
36. Gettel, S. *et al. Correcting Astrophysical Noise in HARPS-N RV Measurements*. Available at http://www.mpia-hd.mpg.de/homes/ppvi/posters/2K024.html (2013).
37. Cegla, H. M., Stassun, K. G., Watson, C. A., Bastien, F. A. & Pepper, J. Estimating stellar radial velocity variability from Kepler and GALEX: implications for the radial velocity confirmation of exoplanets. *Astrophys. J.* **780,** 104 (2014).
38. Bastien, F. A. *et al*. Radial velocity variations of photometrically quiet, chromospherically inactive Kepler stars: a link between RV jitter and photometric flicker. *Astron. J.* **147,** 29 (2014).
39. Barnes, J. R. *et al*. Precision radial velocities of 15 M5–M9 dwarfs. *Mon. Not. R. Astron. Soc.* **439,** 3094–3113 (2014).
40. Pepe, F., Mayor, M. & Rupprecht, G. HARPS: ESO's coming planet searcher. Chasing exoplanets with the La Silla 3.6-m telescope. *Messenger* **110,** 9–14 (2002).
41. Pasquini, L., Cristiani, S., Garcia-Lopez, R., Haehnelt, M. & Mayor, M. CODEX: an ultra-stable high resolution spectrograph for the E-ELT. *Messenger* **140,** 20–21 (2010).
42. Pepe, F. *et al*. ESPRESSO: the next European exoplanet hunter. *Astron. Nachr.* **335,** 8 (2014).
43. Szentgyorgyi, A. *et al*. The GMT-CfA, Carnegie, Catolica, Chicago Large Earth Finder (G-CLEF): a general purpose optical echelle spectrograph for the GMT with precision radial velocity capability. *Proc. SPIE* **8446,** 84461H (2012).
44. Kasting, J. F., Whitmire, D. P. & Reynolds, R. T. Habitable zones around main sequence stars. *Icarus* **101,** 108 (1993).
This paper provides a definition for the habitable zone.
45. Heacox, W. D. in *Fiber Optics in Astronomy* (ed. S. C. Barden) 204–235 (*Astron. Soc. Pacif.*, 1988)
46. Hubbard, E. N., Angel, J. R. P. & Gresham, M. S. Operation of a long fused silica fiber as a link between telescope and spectrograph. *Astrophys. J.* **229,** 1074–1078 (1979).
47. Barden, S. C., Ramsey, L. W. & Truax, R. J. Evaluation of some fiber optical waveguides for astronomical instrumentation. *Publ. Astron. Soc. Pacif.* **93,** 154–162 (1981).
48. Heacox, W. D. & Connes, P. Optical fibers in astronomical instruments. *Astron. Astrophys.* **3,** 169–199 (1992).
This paper contains a complete and detailed discussion of instrumental effects and in particular the use of optical fibres for image scrabbling.
49. Hunter, T. R. & Ramsey, L. W. Scrambling properties of optical fibers and the performance of a double scrambler. *Publ. Astron. Soc. Pacif.* **104,** 1244–1251 (1992).
50. Avila, G., Buzzoni, B. & Casse, M. Fiber characterization and compact scramblers at ESO. *Proc. SPIE* **3355,** 900–904 (1998).
51. Avila, G. & Singh, P. Optical fiber scrambling and light pipes for high accuracy radial velocities measurements. *Proc. SPIE* **7018,** 70184W (2008).
52. Chazelas, B., Pepe, F. & Wildi, F. Optical fibers for precise radial velocities: an update. *Proc. SPIE* **8450,** 845013 (2012).
53. Plavchan, P. P. *et al*. Precision near-infrared radial velocity instrumentation II: noncircular core fiber scrambler. *Proc. SPIE* **8864,** 88640G (2013).
54. Cosentino, R. *et al*. Harps-N: the new planet hunter at TNG. *Proc. SPIE* **8446,** 84461V (2012).
55. Bouchy, F. *et al*. SOPHIE+: first results of an octagonal-section fiber for high-precision radial velocity measurements. *Astron. Astrophys.* **549,** 49 (2013).
56. Mahadevan, S. & Ge, J. The use of absorption cells as a wavelength reference for precision radial velocity measurements in the near-infrared. *Astrophys. J.* **692,** 1590–1596 (2009).
57. Osterman, S. *et al*. A proposed laser frequency comb-based wavelength reference for high-resolution spectroscopy. *Proc. SPIE* **6693,** 66931G (2007).
58. Li, C.-H. *et al*. A laser frequency comb that enables radial velocity measurements with a precision of 1cm s^{-1}. *Nature* **452,** 610–612 (2008).
59. Steinmetz, T. *et al*. Laser frequency combs for astronomical observations. *Science* **321,** 1335–1337 (2008).
60. Schettino, G. *et al*. The Astro-Comb project. *Proc. SPIE* **7808,** 78081Q (2010).
61. Phillips, D. F. *et al*. Calibration of an echelle spectrograph with an astro-comb: a laser frequency comb with very high repetition rate. *Proc. SPIE* **8446,** 844680 (2012).
62. Johnson, A. R. *et al*. Microresonator-based comb generation without an external laser source. *Opt. Express* **22,** 1394 (2014).
63. Wildi, F., Pepe, F. & Chazelas, B. Curto, Lo, G. & Lovis, C. The performance of the new Fabry-Perot calibration system of the radial velocity spectrograph HARPS. *Proc. SPIE* **8151,** 81511F (2011).
64. Schäfer, S. & Reiners, A. Two Fabry-Perot interferometers for high precision wavelength calibration in the near-infrared. *Proc. SPIE* **8446,** 844694 (2012).
65. Halverson, S. *et al*. Development of fiber Fabry-Perot interferometers as stable near-infrared calibration sources for high resolution spectrographs. *Publ. Astron. Soc. Pacif.* **126,** 445–458 (2014).
66. Schwab, C. *et al*. Stabilizing a Fabry-Perot etalon to 3 cm/s for spectrograph calibration. Preprint at http://arxiv.org/abs/1404.0004 (2014).
67. Reiners, A. *et al*. Detecting planets around very low mass stars with the radial velocity method. *Astrophys. J.* **710,** 432–443 (2010).
68. Desort, M., Lagrange, A. M., Galland, F., Udry, S. & Mayor, M. Search for exoplanets with the radial-velocity technique: quantitative diagnostics of stellar activity. *Astron. Astrophys.* **473,** 983–993 (2007).
69. Huélamo, N. *et al*. TW Hydrae: evidence of stellar spots instead of a hot Jupiter. *Astron. Astrophys.* **489,** L9–L13 (2008).
70. Barnes, J. R., Jeffers, S. V. & Jones, H. R. A. The effect of M dwarf starspot activity on low-mass planet detection thresholds. *Mon. Not. R. Astron. Soc.* **412,** 1599–1610 (2011).
71. Oliva, E. *et al*. The GIANO spectrometer: towards its first light at the TNG. *Proc. SPIE* **8446,** 84463T (2012).
72. Quirrenbach, A. *et al*. CARMENES. I: instrument and survey overview. *Proc. SPIE* **8446,** 84460R (2012).
73. Tamura, M. *et al*. Infrared Doppler instrument for the Subaru Telescope (IRD). *Proc. SPIE* **8446,** 84461T (2012).
74. Mahadevan, S. *et al*. The habitable-zone planet finder: a stabilized fiber-fed NIR spectrograph for the Hobby-Eberly Telescope. *Proc. SPIE* **8446,** 84461S (2012).
75. Ge, J. *et al*. High resolution Florida IR silicon immersion grating spectrometer and an M dwarf planet survey. *Proc. SPIE* **8446,** 844630 (2012).
76. Delfosse, X. *et al*. World-leading science with SPIRou – the nIR spectropolarimeter/high-precision velocimeter for CFHT. *Proc. SF2A* 497–508 (2013).
77. Schwab, C., Leon-Saval, S. G., Betters, C. H., Bland-Hawthorn, J. & Mahadevan, S. Single mode, extreme precision Doppler spectrographs. *IAU Proc.* Preprint at http://arxiv.org/abs/1212.4867 (2012).
78. Wright, J. T. *et al*. The frequency of hot Jupiters orbiting nearby solar-type stars. *Astrophys. J.* **753,** 160 (2012).
79. Collier Cameron, A. *et al*. WASP-1b and WASP-2b: two new transiting exoplanets detected with SuperWASP and SOPHIE. *Mon. Not. R. Astron. Soc.* **375,** 951–957

(2007)
80. Bakos, G. Á. et al. HAT-P-1b: a large-radius, low-density exoplanet transiting one member of a stellar binary. *Astrophys. J.* **656,** 552–559 (2007).
81. Alonso, R. *et al*. TrES-1: the transiting planet of a bright K0 V star. *Astrophys. J.* **613,** L153 (2004).
82. Udalski, A. *et al*. The optical gravitational lensing experiment. Search for planetary and low-luminosity object transits in the galactic disk. Results of 2001 Campaign — Supplement. *Acta Astron*. **52,** 115–128 (2002).
83. Konacki, M., Torres, G., Jha, S. & Sasselov, D. D. An extrasolar planet that transits the disk of its parent star. *Nature* **421,** 507–509 (2003).
This paper reports the first discovery of an exoplanet with a ground-based transit survey.
84. Moutou, C. *et al*. CoRoT: harvest of the exoplanet program. *Icarus* **226,** 1625–1634 (2013).
85. Charbonneau, D., Irwin, J., Nutzman, P. & Falco, E. E. The MEarth project to detect habitable super Earth exoplanets. *Bull. Am. Astron. Soc.* **40,** 242 (2008).
86. Charbonneau, D. *et al*. A super-Earth transiting a nearby low-mass star. *Nature* **462,** 891–894 (2009).
87. Bean, J. L., Miller-Ricci Kempton, E. M.-R. & Homeier, D. A ground-based transmission spectrum of the super-Earth exoplanet GJ 1214b. *Nature* **468,** 669–672 (2010).
88. Croll, B. *et al*. Broadband transmission spectroscopy of the super-Earth GJ 1214b suggests a low mean molecular weight atmosphere. *Astrophys. J.* **736,** 78 (2011).
89. Crossfield, I. J. M., Barman, T. & Hansen, B. M. S. High-resolution, differential, near-infrared transmission spectroscopy of GJ 1214b. *Astrophys. J.* **736,** 132 (2011).
90. Kreidberg, L., Bean, J. L., Désert, J.-M. & Benneke, B. Clouds in the atmosphere of the super-Earth exoplanet GJ 1214b. *Nature* **505,** 69–72 (2014).
This paper presents a high-precision medium-resolution transmission spectrum of a super-Earth.
91. Désert, J.-M. *et al*. Observational evidence for a metal rich atmosphere on the super-Earth GJ1214b. *Astrophys. Lett.* **731,** L40 (2011).
92. Charbonneau, D., Brown, T. M., Latham, D. W. & Mayor, M. Detection of planetary transits across a Sun-like star. *Astrophys. J.* **529,** L45 (2000).
93. Henry, G. W., Marcy, G. W., Butler, R. P. & Vogt, S. S. A. Transiting 51 Peg-like planet. *Astrophys. J.* **529,** L41 (2000).
94. Brown, T. M., Charbonneau, D., Gilliland, R. L., Noyes, R. W. & Burrows, A. Hubble space telescope time-series photometry of the transiting planet of HD 209458. *Astrophys. J.* **552,** 699 (2001).
This paper reports on the first observation of an exoplanet transit from space, with the Hubble Space Telescope.
95. Woodgate, B. E. *et al*. The space telescope imaging spectrograph design. *Publ. Astron. Soc. Pacif.* **110,** 1183 (1998).
96. Charbonneau, D., Brown, T. M., Noyes, R. W. & Gilliland, R. L. Detection of an extrasolar planet atmosphere. *Astrophys. J.* **568,** 377 (2002).
97. Vidal-Madjar, A. *et al*. An extended upper atmosphere around the extrasolar planet HD 209458b. *Nature* **422,** 143–146 (2003).
98. Pont, F. *et al*. Hubble Space Telescope time-series photometry of the planetary transit of HD 189733: no moon, no rings, starspots. *Astron. Astrophys.* **476,** 1347 (2007).
99. Fazio, G. G. *et al*. The Infrared Array Camera (IRAC) for the Spitzer Space Telescope. *Astrophys. J. Suppl. Ser.* **154,** 10 (2004).
100. Charbonneau, D. *et al*. Detection of thermal emission from an extrasolar planet. *Astrophys. J.* **626,** 523 (2005).
101. Deming, D., Seager, S., Richardson, L. J. & Harrington, J. Infrared radiation from an extrasolar planet. *Nature* **434,** 740–743 (2005).
102. Knutson, H. A. *et al*. A map of the day–night contrast of the extrasolar planet HD 189733b. *Nature* **447,** 183–186 (2007).
103. Richardson, L. J., Harrington, J., Seager, S. & Deming, D. A Spitzer infrared radius for the transiting extrasolar planet HD 209458b. *Astrophys. J.* **649,** 1043 (2006).
104. Ehrenreich, D. *et al*. A Spitzer search for water in the transiting exoplanet HD 189733b. *Astrophys. J.* **668,** L179 (2007).
105. Beaulieu, J. P., Carey, S., Ribas, I. & Tinetti, G. Primary transit of the planet HD 189733b at 3.6 and 5.8 μm. *Astrophys. J.* **677,** 1343 (2008).
106. Désert, J.-M. *et al*. Search for carbon monoxide in the atmosphere of the transiting exoplanet HD 189733b. *Astrophys. J.* **699,** 478 (2009).
107. Thompson, R. I. NICMOS: the next U.S. infrared space mission. *Proc. SPIE* **2198,** 1202–1213 (1994).
108. Swain, M. R., Vasisht, G. & Tinetti, G. The presence of methane in the atmosphere of an extrasolar planet. *Nature* **452,** 329 (2008).
109. Sing, D. K. *et al*. Transit spectrophotometry of the exoplanet HD 189733b. I. Searching for water but finding haze with HST NICMOS. *Astron. Astrophys.* **505,** 891–899 (2009).
110. Gibson, N. P., Pont, F. & Aigrain, S. A new look at NICMOS transmission spectroscopy of HD 189733, GJ-436 and XO-1: no conclusive evidence for molecular features. *Mon. Not. R. Astron. Soc.* **411,** 2199 (2011).
This paper explores the impact of instrumental systematics in transmission spectroscopy, which can lead to false-positive detections.
111. Houck, J. R. *et al*. The Infrared Spectrograph (IRS) on the Spitzer Space Telescope. *Astrophys. J. Suppl. Ser.* **154,** 18–24 (2004).
112. Grillmair, C. J. *et al*. A Spitzer spectrum of the exoplanet HD 189733b. *Astrophys. J.* **658,** L115 (2007).
113. Grillmair, C. J. *et al*. Strong water absorption in the dayside emission spectrum of the planet HD 189733b. *Nature* **456,** 767–769 (2008).
114. Demory, B.-O. *et al*. Detection of a transit of the super-Earth 55 Cancri e with warm Spitzer. *Astron. Astrophys.* **533,** 114 (2011).
115. Van Grootel, V. *et al*. Transit confirmation and improved stellar and planet parameters for the super-Earth HD 97658 b and its host star. *Astrophys. J.* **796,** 2 (2014).
116. Snellen, I. A. G., Albrecht, S., de Mooij, E. J. W. & Le Poole, R. S. Ground-based detection of sodium in the transmission spectrum of exoplanet HD 209458b. *Astron. Astrophys.* **487,** 357 (2008).
This paper reports the first detection of an exoplanetary atmosphere from the ground, with a high-resolution spectrograph installed at the Subaru telescope.
117. Narita, N. *et al*. Subaru HDS transmission spectroscopy of the transiting extrasolar planet HD 209458b. *Publ. Astron. Soc. Jpn* **57,** 471 (2005).
118. Sing, D. K. *et al*. Gran Telescopio Canarias OSIRIS transiting exoplanet atmospheric survey: detection of potassium in XO-2b from narrowband spectrophotometry. *Astron. Astrophys.* **527,** 73 (2011).
119. Colon, K. D. *et al*. Measuring potassium in exoplanet atmospheres with the OSIRIS tunable filter. *RevMexAA (Serie de Conferencias)* **42,** 1–2 (2013).
120. Snellen, I. A. G., de Kok, R. J., de Mooij, E. J. W. & Albrecht, S. The orbital motion, absolute mass and high-altitude winds of exoplanet HD209458b. *Nature* **465,** 1049–1051 (2010).
121. Birkby, J. L. *et al*. Detection of water absorption in the dayside atmosphere of HD 189733 b using ground-based high-resolution spectroscopy at 3.2 microns. *Mon. Not. R. Astron. Soc.* **436,** L35 (2013).
122. Lockwood, A. C., Johnson, J. A. & Bender, C. F. Near-IR direct detection of water vapor in τ Boötis b. *Astrophys. Lett.* **783,** L29 (2014).
123. Brogi, M. *et al*. The signature of orbital motion from the dayside of the planet τ Boötis b. *Nature* **486,** 502–504 (2012).
124. Lagrange, A.-M. *et al*. A probable giant planet imaged in the β Pictoris disk. VLT/NaCo deep L'-band imaging. *Astron. Astrophys.* **493,** L21 (2009).
This paper reports the near-infrared detection of the giant exoplanet β Pictoris b from adaptive-optics high-contrast observations with the NACO instrument on the VLT.
125. Snellen, I. *et al*. The fast spin-rotation of the young extrasolar planet β Pictoris b. *Nature* **509,** 63–65 (2014).
This paper details how ground-based, high-resolution spectroscopy can be used to probe the atmosphere of a directly imaged exoplanet and measure its spin-rotation.
126. Green, J. C. Cosmic origins spectrograph. *Proc. SPIE* **4498,** 229–238 (2001).
127. Kimble, R. A., MacKenty, J. W., O'Connell, R. W. & Townsend, J. A. Wide Field Camera 3: a powerful new imager for the Hubble Space Telescope. *Proc. SPIE* **7010,** 70101E (2008).
128. Linsky, J. L. *et al*. Observations of mass loss from the transiting exoplanet HD 209458b. *Astrophys. J.* **717,** 1291 (2010).
129. Lecavelier des Etangs, A. *et al*. Temporal variations in the evaporating atmosphere of the exoplanet HD 189733b. *Astron. Astrophys.* **543,** L4 (2012).
130. Bourrier, V. *et al*. Atmospheric escape from HD 189733b observed in HI Lyman-α: detailed analysis of HST/STIS September 2011 observations. *Astron. Astrophys.* **551,** A63 (2013).
131. Ehrenreich, D. *et al*. Hint of a transiting extended atmosphere on 55 Cancri b. *Astron. Astrophys.* **547,** 18 (2012).
132. Fossati, L. *et al*. Metals in the exosphere of the highly irradiated planet WASP-12b. *Astrophys. Lett.* **714,** L222 (2010).
133. Kulow, J. R., France, K., Linsky, J. & Loyd, R. O. P. Lyα Transit spectroscopy and the neutral hydrogen tail of the hot Neptune GJ 436b. *Astrophys. J.* **786,** 132 (2014).
134. Huitson, C. M., Sing, D. K., Vidal-Madjar, A., Ballester, G. E. & Lecavelier des Etangs, A. Temperature-pressure profile of the hot Jupiter HD 189733b from HST sodium observations: detection of upper atmospheric heating. *Mon. Not. R. Astron. Soc.* **422,** 2477 (2012).
135. Evans, T. M. *et al*. The deep blue color of HD 189733b: albedo measurements with Hubble Space Telescope/Space Telescope imaging spectrograph at visible wavelengths. *Astrophys. Lett.* **772,** L16 (2013).
136. Berta, Z. K. *et al*. The flat transmission spectrum of the super-Earth GJ1214b from Wide Field Camera 3 on the Hubble Space Telescope. *Astrophys. J.* **747,** 35 (2012).
137. Deming, D. *et al*. Infrared transmission spectroscopy of the exoplanets HD 209458b and XO-1b using the Wide Field Camera-3 on the Hubble Space Telescope. *Astrophys. J.* **774,** 95 (2013).
138. Mandell, A. *et al*. Exoplanet transit spectroscopy using WFC3: WASP-12 b, WASP-17 b, and WASP-19 b. *Astrophys. J.* **779,** 128 (2013).
139. Knutson, H. A., Benneke, B., Deming, D. & Homeier, D. A featureless transmission spectrum for the Neptune-mass exoplanet GJ 436b. *Nature* **505,** 66–68 (2014).
140. Ranjan, S. *et al*. Atmospheric characterization of 5 hot Jupiters with Wide Field Camera 3 on the Hubble Space Telescope. *Astrophys. J.* **785,** 148 (2014).
141. Gibson, N. P. *et al*. Probing the haze in the atmosphere of HD 189733b with HST/WFC3 transmission spectroscopy. *Mon. Not. R. Astron. Soc.* **422,** 753 (2012).
142. Knutson, H. A. *et al*. Hubble Space Telescope near-IR transmission spectroscopy of the super-Earth HD 97658b. Preprint at http://arxiv.org/abs/1403.4602 (2014).
143. Ehrenreich, D. *et al*. Near-infrared transmission spectrum of the warm-Uranus GJ 3470b with the Wide Field Camera-3 on the Hubble Space Telescope. Preprint at http://arxiv.org/abs/1405.1056 (2014).
144. Marois, C. *et al*. Direct imaging of multiple planets orbiting the star HR 8799.

Science **322,** 1348–1352 (2008).
This paper reports on the discovery of three planetary companions, directly imaged in the near-infrared at two different epochs with the adaptive-optics systems at the Gemini and Keck telescopes, and the corresponding facility near-infrared cameras.
145. Kalas, P. *et al*. Optical images of an exosolar planet 25 light-years from Earth. *Science* **322,** 1345–1348 (2008).
146. Kalas, P., Graham, J. R., Fitzgerald, M. P. & Clampin, M. HST/STIS imaging of Fomalhaut: new main belt structure and confirmation of Fomalhaut b's eccentric orbit. *Proc. IAU* **8,** 204–207 (2014).
147. Lagrange, A.-M. *et al*. Constraining the orbit of the possible companion to β Pictoris. New deep imaging observations. *Astron. Astrophys.* **506,** 927 (2009).
148. Lagrange, A.-M. *et al*. A giant planet imaged in the disk of the young star β Pictoris. *Science* **329,** 57 (2010).
149. Quanz, S. P. *et al.* First results from Very Large Telescope NACO apodizing phase plate: 4 μm images of the exoplanet β Pictoris b. *Astrophys. Lett.* **722,** L49 (2010).
150. Smith, B. A. & Terrile, R. J. A circumstellar disk around β Pictoris. *Science* **226,** 1421–1424 (1984).
151. Chauvin, G. *et al*. A giant planet candidate near a young brown dwarf. *Astron. Astrophys.* **425,** L29–L32 (2004).
This paper reports the first direct detection of a planetary-mass object, orbiting a brown dwarf, with the NACO instrument on the VLT.
152. Chabrier, G., Johansen, A., Janson, M. & Rafikov, R. Giant planet and brown dwarf formation. Preprint at http://arxiv.org/abs/1401.7559 (2014).
153. Davies, R. & Kasper, M. Adaptive optics for astronomy. *Annu. Rev. Astron. Astrophys.* **50,** 305–351 (2012).
154. Nielsen, E. L. & Close, L. M. A uniform analysis of 118 stars with high-contrast imaging: long-period extrasolar giant planets are rare around Sun-like stars. *Astrophys. J.* **717,** 878–896 (2010).
155. Fusco, T. *et al*. Integration of SAXO, the VLT-SPHERE extreme AO: final performance. *Proc. Third AO4ELT Conf*. http://dx.doi.org/10.12839/AO4ELT3.13327 (2013).
156. Macintosh, B. *et al*. The Gemini Planet Imager: first light. *Proc. Natl Acad. Sci. USA* Preprint at http://arxiv.org/abs/1403.7520 (2014).
157. Close, L. *et al*. Into the blue: AO science in the visible with MagAO. *Proc. Third AO4ELT Conf*. http://dx.doi.org/10.12839/AO4ELT3.13387 (2013).
158. Marois, C., Lafrenière, D., Doyon, R., Macintosh, B. & Nadeau, D. Angular differential imaging: a powerful high-contrast imaging technique. *Astrophys. J.* **641,** 556 (2006).
159. Amara, A. & Quanz, S. P. PYNPOINT: an image processing package for finding exoplanets. *Mon. Not. R. Astron. Soc.* **427,** 948–955 (2012).
160. Quanz, S. P. *et al*. Resolving the inner regions of circumstellar discs with VLT/NACO polarimetric differential imaging. *Messenger* **146,** 25–27 (2011).
161. Milli, J. *et al*. Prospects of detecting the polarimetric signature of the Earth-mass planet α Centauri B b with SPHERE/ZIMPOL. *Astron. Astrophys.* **556,** 64 (2013).
162. Crepp, J. R. *et al*. Speckle suppression with the Project 1640 Integral Field Spectrograph. *Astrophys. J.* **729,** 132 (2011).
163. Ireland, M. J. Phase errors in diffraction-limited imaging: contrast limits for sparse aperture masking. *Mon. Not. R. Astron. Soc.* **433,** 1718–1728 (2013).
164. Kenworthy, M. A. *et al*. First on-sky high-contrast imaging with an apodizing phase plate. *Astrophys. J.* **660,** 762–769 (2007).
165. Mawet, D. *et al*. L'-band AGPM vector vortex coronagraph's first light on VLT/NACO. Discovery of a late-type companion at two beamwidths from an F0V star. *Astron. Astrophys.* **552,** L13 (2013).
166. Guyon, O. Phase-induced amplitude apodization of telescope pupils for extrasolar terrestrial planet imaging. *Astron. Astrophys.* **404,** 379–387 (2003).
167. Mawet, D. *et al*. Review of small-angle coronagraphic techniques in the wake of ground-based second-generation adaptive optics systems. *Proc. SPIE* **8442,** 844204 (2012).
168. Bailey, V. *et al*. The large binocular telescope interferometer and adaptive optics system: on-sky performance and results. *Proc. IAU* **8,** 26–27 (2014).
169. Codona, J. L. & Kenworthy, M. Focal plane wavefront sensing using residual adaptive optics speckles. *Astrophys. J.* **767,** 100 (2013).
170. Quanz, S. P., Crossfield, I., Meyer, M. R., Schmalzl, E. & Held, J. Direct detection of exoplanets in the 3–10 micron range with E-ELT/METIS. *Int. J. Astrobiol*. Preprint at http://arxiv.org/abs/1404.0831 (2014).
171. Sozzetti, A. *et al*. Astrometric detection of giant planets around nearby M dwarfs: the Gaia potential. *Mon. Not. R. Astron. Soc.* **437,** 497–509 (2014).
172. Sahlmann, J. *et al*. Narrow-angle astrometry with PRIMA. *Proc. SPIE* **8445,** 84450S1 (2012).
173. Howell, S. B. *et al*. The K2 mission: characterization and early results. *Publ. Astron. Soc. Pacif*. Preprint at http://arxiv.org/abs/1402.5163 (2014).
174. Ricker, G. R. *et al*. The Transiting Exoplanet Survey Satellite (TESS). *Bull. Am. Astron. Soc.* **41,** 193 (2009).
175. Rauer, H. *et al*. The PLATO 2.0 mission. *Exp. Astron*. Preprint at http://arxiv.org/abs/1310.0696 (2013).
176. Snellen, I. *et al*. Ground-based search for the brightest transiting planets with Multi-site All Sky Camera - MASCARA. *Proc. SPIE* **8444,** 844401 (2012)
177. CHEOPS Study Team. *CHEOPS Definition Study Report (Red Book)* (ESA, 2013).
178. Broeg, C. *et al*. CHEOPS: A transit photometry mission for ESA's small mission programme. *EPJ Web Conf.* **47,** 03005 (2013).
179. Snellen, I. A. G., de Kok, R. J., le Poole, R., Brogi, M. & Birkby, J. Finding extraterrestrial life using ground-based high-dispersion spectroscopy. *Astrophys. J.* **764,** 182 (2013).
180. Vogt, S. S. The Lick Observatory Hamilton Echelle Spectrometer. *Publ. Astron. Soc. Pacif.* **99,** 1214–1228 (1987).
181. Horton, A. *et al*. CYCLOPS2: the fibre image slicer upgrade for the UCLES high resolution spectrograph. in *Proc. SPIE* **8446,** 84463A (2012).
182. Dekker, H., D'Odorico, S., Kaufer, A., Delabre, B. & Kotzlowski, H. Design, construction, and performance of UVES, the echelle spectrograph for the UT2 Kueyen Telescope at the ESO Paranal Observatory. *Proc. SPIE* **4008,** 534 (2000).
183. Tull, R. G. High-resolution fiber-coupled spectrograph of the Hobby-Eberly Telescope. In *Proc. SPIE* **3355,** 387 (1998).
184. Noguchi, K. *et al*. High Dispersion Spectrograph (HDS) for the Subaru Telescope. *Publ. Astron. Soc. Jpn.* **54,** 855–864 (2002).
185. Kaufer, A. *et al*. Commissioning FEROS, the new high-resolution spectrograph at La-Silla. *Messenger* **95,** 8–12 (1999).
186. Bernstein, R., Shectman, S. A., Gunnels, S. M., Mochnacki, S. & Athey, A. E. MIKE: a Double Echelle Spectrograph for the Magellan Telescopes at Las Campanas Observatory. *Proc. SPIE* **4841,** 1694 (2003).
187. Bouchy, F. & Team, S. in *Proc. Colloquium of the Tenth Anniversary of 51 Peg-b* 319–325 http://www.obs-hp.fr/www/pubs/Coll51Peg/proceedings.html (2006).
188. Kaeufl, H.-U. *et al*. CRIRES: a high-resolution infrared spectrograph for ESO's VLT. *Proc. SPIE* **5492,** 1218 (2004).
189. Crane, J. D. *et al*. The Carnegie Planet Finder Spectrograph: integration and commissioning. *Proc. SPIE* **7735,** 773553 (2010).
190. Chakraborty, A. *et al*. First light results from PARAS: the PRL Echelle Spectrograph. *Proc. SPIE* **7735,** 77354N (2010).
191. Aceituno, J. *et al*. CAFE: Calar Alto Fiber-fed Échelle spectrograph. *Astron. Astrophys.* **552,** 31 (2013).
192. Schwab, C., Spronck, J. F. P., Tokovinin, A. & Fischer, D. A. Design of the CHIRON high-resolution spectrometer at CTIO. *Proc. SPIE* **7735,** 77354G (2010).
193. Vogt, S. S. *et al*. APF - The Lick Observatory Automated Planet Finder. *Publ. Astron. Soc. Pacif.* Preprint at http://arxiv.org/abs/1402.6684 (2014).
194. Ge, J. *et al*. Design and performance of a new generation, compact, low cost, very high Doppler precision and resolution optical spectrograph. *Proc. SPIE* **8446,** 84468R (2012).
195. Bramall, D. G. *et al*. The SALT HRS spectrograph: instrument integration and laboratory test results. *Proc. SPIE* **8446,** 84460A (2012).
196. Strassmeier, K. G. *et al*. PEPSI: the Potsdam Echelle Polarimetric and Spectroscopic Instrument for the LBT. *Proc. SPIE* **7014,** 70140N (2008).
197. Brown, T. M., Noyes, R. W., Nisenson, P., Korzennik, S. G. & Horner, S. The AFOE: a spectrograph for precise Doppler studies. *Publ. Astron. Soc. Pacif.* **106,** 1285–1297 (1994).
198. Tull, R. G., MacQueen, P. J., Sneden, C. & Lambert, D. L. The high-resolution cross-dispersed echelle white-pupil spectrometer of the McDonald Observatory 2.7-m telescope. *Publ. Astron. Soc. Pacif.* **107,** 251–264 (1995).
199. Schneider, J., Dedieu, C., Le Sidaner, P., Savalle, R. & Zolotukhin, I. Defining and cataloging exoplanets: the exoplanet.eu database. *Astron. Astrophys.* **532,** A79 (2011).

Acknowledgements D.E. would like to dedicate this article to the memory of STIS Principal Investigator Bruce Woodgate who passed away in April 2014. This work has been carried out within the frame of the National Centre for Competence in Research 'PlanetS' supported by the Swiss National Science Foundation (SNSF). The authors acknowledge the financial support of the SNSF.

Author Information Reprints and permissions information is available at www.nature.com/reprints. The authors declare no competing financial interests. Readers are welcome to comment on the online version of this paper at go.nature.com/azn8hn. Correspondence should be addressed to F.P. (Francesco.Pepe@unige.ch).